Nanostructures Inside Colloidal Particles of Block Copolymer/Homopolymer Blends

Seog-Jin Jeon,[†] Gi-Ra Yi,*[,‡] Chong Min Koo,[§] and Seung-Man Yang*[,†]

National Creative Research Initiative Center for Integrated Optofluidic Systems and Department of Chemical and Biomolecular Engineering, Korea Advanced Institute of Science and Technology, Daejeon 305-701, Korea, Nano-Bio System Research Team, Seoul Center, Korea Basic Science Institute, Seoul 136-713, Korea, Performance Polymer R&D, LG Chem Research Park, Daejeon 305-380, Korea

Received June 2, 2007; Revised Manuscript Received August 7, 2007

ABSTRACT: Colloidal spheres with unique internal morphologies were prepared by blending symmetrical poly(styrene)-*block*-poly(butadiene) (PS-*b*-PB) and polystyrene homopolymer (*h*PS) in emulsion droplets and carrying out subsequent solvent evaporation. We found various unprecedented microphases in these spherically confining geometries that depend on the ratio (r) of the molecular weight of *h*PS relative to that of the PS block of PS-*b*-PB and the ratio of the diameter (D) of the emulsion drop to the feature spacing (L_0) of the phase-separated periodic domains. In particular, the effect of spherical confining geometry was pronounced for $D/L_0 < 15$, in which directionally oriented structures such as helices and hoops were observed. For $r < 1$, the PB domains exhibit transitions between morphological microphases of lamellae, perforated lamellae, cylinders, and spheres, in that order, as the weight fraction of *h*PS (ϕ) is increased. The lamellae or perforated lamellae are ordered in concentric shells. Interestingly, cylindrical domains of PB blocks consisting of circular helices or stacked hoops were observed for $0.38 \leq \phi \leq 0.54$, in which the particle shape is slightly deformed from spherical to accommodate the ordered regular packing of the hoops and helices. For $r \sim 2$, concentric spherical lamellae are produced for ϕ up to 0.30, above which macrophase separation occurs and the spherical lamellae are either nonconcentric or deformed into a domelike structure. For $r \sim 4$, an onion-like structure is present for the entire range of ϕ, with a lamellar spacing that is nearly independent of ϕ due to macrophase separation. In particular, for $r \sim 1$, spherical lamellar morphology is present up to $\phi = 0.30$, and complex anomalous structures such as multiply jointed hoops are present for $\phi \geq 0.32$ because of the combined effects of micro- and macrophase separations.

1. Introduction

Block copolymers have isotropic (e.g., double-gyroid, body-centered cubic) or anisotropic (e.g., lamellar, hexagonal) morphologies depending on their composition, segment−segment interaction parameters, and degree of polymerization.[1,2] Over the past decade, block copolymer thin films have been studied extensively due to their potential applications as alternative nonlithographic tools for nanoscale patterning in nanoelectronics,[3] biological assays,[4] and high-density storage.[5] The key to the use of block copolymers in such applications is the control of the orientation and lateral order of the microdomains in the thin films. For instance, the orientation of lamellar structures can be controlled by changing the surface properties of the substrate or the gap between two substrates.[6−8] Moreover, to enhance or control the lateral order of microdomains in block copolymers, patterned substrates or cylindrical pores in anodized alumina membranes have been used as confining geometries.[9−12] Theories of two-dimensional (2D) confinement in cylindrical pores have recently predicted various unusual morphologies such as single helices, double helices, and meshes.[13−17]

Likewise, three-dimensional (3D) confining geometries are useful for controlling the 3D morphology of block copolymers. In particular, spherical confinement has been shown to produce multilayered structures or other morphologies that are of practical importance in a broad range of applications, including the production of impact-resistant polymers, composite materials, catalytic supports, coatings, and adhesives.[18] Further, dyed multilayer particles have been used in high-density three-dimensional optical data storage and security data encryption.[19] Moreover, structured spheres with periodic radial variation of the refractive index have attracted much attention due to their potential uses as spherical dielectric resonators in cavity quantum electrodynamics, optical switches, and limiters.[20,21]

Structured block copolymer particles were originally prepared by using the spherical confinement of aerosol droplets, with final diameters ranging from submicrometers to a few micrometers after the complete removal of the solvent from the aerosol droplets.[22] However, the internal structures of airborne block copolymer particles are typically unclear because of significant overlap between the neighboring domains, which is due to the fast removal of the solvent from the aerosol droplets of block copolymer solution. In addition, the interfacial property contrast of the air−liquid interface of aerosol droplets cannot be controlled as well as is possible for the liquid−liquid interface of emulsion droplets. Emulsion droplets were recently used as confining geometries in the synthesis of block copolymer microspheres with cylindrical, spherical, and lamellar morphologies by carrying out the simple evaporation-induced microphase separation of diblock copolymers in the presence of homopolymers inside the emulsion droplets.[23] In this case, the microdomains of spheres, cylinders, and lamellae were structured in concentric arrangements due to the external spherical confinement provided by the emulsion droplets. In that study, however, the ratio of the particle diameter to the feature spacing (D/L_0)

* Corresponding authors. E-mail: smyang@kaist.ac.kr (S.-M.Y.); yigira@kbsi.re.kr (G.-R.Y.).
† Korea Advanced Institute of Science and Technology.
‡ Korea Basic Science Institute.
§ LG Chem Research Park.

10.1021/ma0712302 CCC: $37.00
Published on Web 10/11/2007

Table 1. Physical Properties of PS-*b*-PB and *h*PS

polymers	M_p [g/mol]	M_w/M_n	f_s [wt %]
PS-*b*-PB	85 000	1.05	55
2k-*h*PS	1920	1.06	100
10k-*h*PS	9950	1.03	100
19k-*h*PS	18 800	1.01	100
44k-*h*PS	44 000	1.08	100
96k-*h*PS	95 800	1.06	100
200k-*h*PS	213 000	1.08	100

was more than 20, which was too large for the curvature-induced directional microphase orientation to be observed.

In the present study, we prepared nanostructured colloidal particles of symmetrical poly(styrene)-*b*-poly(butadiene) (PS-*b*-PB) swelled with polystyrene homopolymers (*h*PS) in oil-in-water emulsion droplets and investigated the internal microphases resulting from strong spherical confinement using a cryo-ultramicrotome and transmission electron microscopy. The sizes of the block copolymer particles were of submicrometer scale, and the ratio D/L_0 of the length scales was kept below 20, which is much smaller than those of previous studies. For these low values of D/L_0, the effects of spherical confinement on the morphology of symmetrical PS-*b*-PB in the presence of *h*PS are significant, and we were able to observe unprecedented ordered and deformed structures. In particular, for a given block ratio, we found that the weight fraction ϕ of *h*PS, the particle size, and the ratio r of the molecular weight of *h*PS to that of the PS-block in the PS-*b*-PB block copolymer determine the microphase structures of the PS-*b*-PB block copolymer particles.

2. Experimental Section

2.1. Chemicals. Poly(styrene)-*block*-poly(butadiene) diblock copolymer (PS-*b*-PB) was synthesized by anionic polymerization. Polystyrene homopolymers (*h*PS) with six different molecular weights were purchased from Fluka and Aldrich. The physical properties of the PS-*b*-PB diblock copolymers and *h*PS are summarized in Table 1. The prefix in front of *h*PS (e.g., 96k in 96k-*h*PS) indicates the approximate molecular weight. Toluene (Merck) was used as a solvent for the polymers. A triblock poly(ethylene oxide)−poly(propylene oxide)−poly(ethylene oxide) copolymer (Pluronic F108, BASF) was used as a surfactant. Aqueous 2% osmium tetraoxide (OsO_4, Polysciences) was used to selectively stain unsaturated blocks of the block copolymers for transmission electron microscopy (TEM) imaging. An epoxy resin (EpoFix kit, Struers) was used to prepare specimens for the cross-sectional TEM imaging.

2.2. Generation of the Block Copolymer Particles. A 1 wt % polymer solution was prepared by dissolving PS-*b*-PB and *h*PS in toluene, and 1 mL of the polymer solution was emulsified into 8 mL of distilled water containing 1 wt % Pluronic F108 by using a homogenizer (Heidolph; DIAX900) at 22 000 rpm for 1 min. The droplet toluene phase was removed from the aqueous emulsion by evaporation in a vacuum oven. Before evaporation, 30 mL of distilled water was added to the 9 mL of aqueous emulsion to prevent the continuous aqueous phase from drying out prior to the complete evaporation of toluene. For the evaporation of toluene, the sample was kept in an oven at 95 °C for 2 h, and subsequently the toluene and water mixture vapor was trapped under vacuum conditions for 30 min. Detailed procedure for the solvent removal has been reported in the literature.[23] Annealing the sample at 95 °C for 2.5 h was then used to completely remove the toluene solvent, leaving behind nanostructured colloidal particles of PS-*b*-PB dispersed in the aqueous medium. The dispersion was washed with distilled water to remove the surfactant Pluronic F108 by repeated centrifugation at 12 000 rpm for 10 min.

2.3. Electron Microscopy. The internal microphase structures of the block copolymer particles were investigated with TEM. After dilution with distilled water and sonication for 10 min, the particle dispersion was dropped onto a Formvar/Carbon coated TEM grid and dried completely. To obtain proper contrast between the PS and PB phases under TEM, the PB phase was selectively stained with the vapor from an aqueous 2 wt % OsO_4 solution for 2 h.

When the internal structures of the block copolymer particles were not clear in the TEM images due to significant overlap of the PB domains, cross-sectional images were obtained, in particular for the mesophase and cylinder domains. To obtain these images, the OsO_4 stained particles were embedded in an epoxy resin and solidified at room temperature for 24 h. Ultrathin sections (50−70 nm) of the block copolymer particles were prepared at a low temperature (−120 °C) using a diamond knife (Drukker) and a cryo-ultramicrotome (Leica, EMFCS) and mounted on a Formvar/Carbon coated TEM grid by using a loop. The prepared samples were examined in the bright-field mode using a Philips CM20 conventional TEM operated at 200 kV.

The diameter of blend particles and the lamellar spacing were measured by using an image processing software (Gatan, DigitalMicrograph) for the calculation of D/L_0. To investigate the increment of L_0 according to r and ϕ, the lamellar spacing of more than 20 particles were measured and the average lamellar spacing and the standard error were calculated by a graphic and analysis software (OriginLab, Origin 6.0).

3. Results and Discussion

3.1. Phase Behavior of the Blend Microspheres for $r < 1$. We begin with the phase behavior of the PS-*b*-PB block copolymers in the presence of polystyrene homopolymers (2k-*h*PS, 10k-*h*PS, and 19k-*h*PS) with three different molecular weights, which correspond to molecular weight ratios of $r = 0.04$, 0.21, and 0.40, respectively. The present results show that block copolymer particles that are prepared in the presence of high volume fractions of low-molecular-weight *h*PS are deformable and easily lose their sphericity. This is because low-molecular-weight *h*PS is not fully entangled but behaves like a plasticizer for the styrene blocks. For example, block copolymer particles containing 2k-*h*PS (i.e., for $r = 0.04$) with $\phi \geq 0.8$ are easily deformed into oblates after drying. However, when the molecular weight of *h*PS is as large as 10 000, i.e., for $r = 0.21$, the block copolymer particles retain their spherical shape after drying for the entire range of ϕ.

The effect of *h*PS on the internal microphase morphology of the spherical block copolymer particles was explored by varying the weight fraction of *h*PS when the molecular weight of *h*PS was small compared with that of PS blocks (i.e., $r < 1$). In this wet-brush regime, *h*PS tends to penetrate into the polymeric brushes that are formed by the PS blocks at the microdomain interfaces. The penetrated *h*PS swells the PS blocks and increases interfacial area per block.[24−27] As we shall see shortly, phase transition occurs toward microphases with higher mean curvatures at the interfaces (e.g., from lamellae to spheres) as the *h*PS content increases. First, we examined the case in which the ratio D/L_0 of the particle diameter to the feature spacing was large, i.e., the confinement effects are moderate. For 10k-*h*PS with $\phi \leq 0.28$, an onion-like concentric lamellar morphology develops, as shown in Figure 1a. Onion-like lamellar structures were also observed for 2k-*h*PS and 19k-*h*PS when ϕ was smaller than 0.28. The outermost layers were found to be filled with polymer blocks, which lower the surface energy at the oil-in-water emulsion interface between the toluene phase containing polymer and the aqueous phase containing surfactant, as reported by the Okubo group.[28] In the present case, the PS blocks form the outermost layers of the PS-*b*-PB block copolymer particles. Interestingly, for $0.30 \leq \phi \leq 0.36$ with 10k-*h*PS, concentric perforated lamellar (henceforth, PL) morphologies form, as shown in the TEM images in Figure 1b,c. The cross-sectional TEM image in Figure 1c clearly shows the

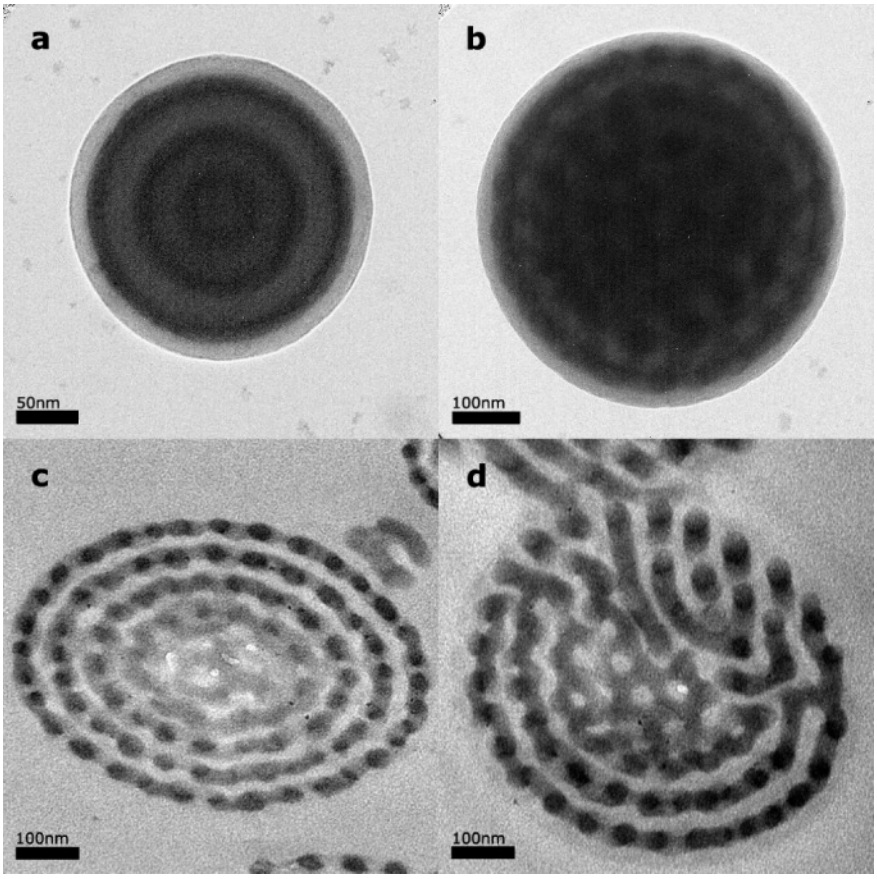

Figure 1. Blend particles of PS-*b*-PB and 10k-*h*PS. (a) Lamellar morphology for $\phi = 0.2$ ($D/L_0 \sim 6.5$). (b) Perforated lamellar (PL) morphology for $\phi = 0.32$ ($D/L_0 \sim 11.5$). (c) Thin section of a particle similar to the particle shown in (b) confirms the PL morphology ($D/L_0 \geq 10$). (d) Interconnection between layers is observed for $D/L_0 \geq 10$.

formation of the PL phase. For 2k-*h*PS and 19k-*h*PS, the PL phase was observed over approximately the same range of ϕ as for 10k-*h*PS. Similar PL phases also formed when PS-*b*-PB and *h*PS were blended for $0.35 \leq \phi \leq 0.40$ in the absence of any geometrical confinement.[29] However, note that when D/L_0 is larger than 10, most particles exhibit an interconnected cylinder structure together with PL morphology, as shown in Figure 1d. The coexistence of the PL and cylinder phases is due to the relatively weak geometrical confinement. Okubo and co-workers examined the internal microphase morphology of spherical particles prepared from blends of PS-*b*-PMMA and *h*PS for a molecular weight ratio of $r = 0.09$ and found that a gyroid phase forms with a cylinder phase in the PS-*b*-PMMA particles for $\phi \sim 0.2$.[23] As mentioned above, the PS-*b*-PMMA particles were so large ($D/L_0 \geq 20$) that the spherical confinement was not significant. The insufficient confinement was responsible for the coexistence of two different microphases in the blend particles of PS-*b*-PMMA and *h*PS.

However, we found that as D/L_0 becomes smaller, a single pure microphase forms inside the blend particles of PS-*b*-PB and *h*PS due to strong capillary forces arising from large interface curvatures. The orientation of microdomains is defined primarily by the emulsion interface in the limit of small D/L_0. The general features can be seen in the TEM images in Figure 2a, which contain blend particles of various sizes. It can be clearly seen in the left bottom corner of the TEM image that small blend particles (<200 nm, $D/L_0 = 2-3$) contain a microphase intrastructure composed of a few layered lamellae because microphase transition is limited due to strong compressive capillary forces for high curvature interfaces. Further, the TEM images of the ultramicrotomed particles in Figure 2b,c show that the 140 nm particles contain one and a half bilayers with PB as the core for $D/L_0 \sim 3$ (Figure 2b), and the 240 nm particles contain two bilayers with PS as the core for $D/L_0 \sim 4$ (Figure 2c). The internal morphologies are schematically drawn in Figure 2d for illustrative purposes. Interestingly, of the two lamellae of the 240 nm particles, only the internal lamellar layer is perforated. If the particle size is further increased, a pure PL morphology develops, as shown in Figure 2e, of which schematic illustration is reproduced in Figure 2f. Therefore, the capillary forces associated with the curvature of confining geometry are the dominant effect on the internal morphology, especially in the limit of small D/L_0.

As the content of *h*PS is increased above the limit of lamellar (or perforated lamellar) structure, a phase transition is observed. For example, cylinders of PB form inside the spherical PS-*b*-PB and *h*PS blend particles when the weight fraction of 10k-*h*PS is in the range $0.38 \leq \phi \leq 0.54$. Several theoretical and experimental studies of the microphase behavior of block copolymers in cylindrical pores have recently been conducted and found that ordered cylinders consisting of circular helices and stacked hoops form for $0.5 \leq D/L_0 \leq 5.0$.[9−11,14−17] We also observed circular helices in a spherical confining geometry for $0.38 \leq \phi \leq 0.48$, and the resulting TEM images are reproduced in Figure 3 for various D/L_0 ratios. In the case of spherical confinement, the range of D/L_0 in which helices or stacked hoops are observed is different from that for the cylindrical confinement case. For $\phi = 0.4$, only a lamellar layer or a spherical domain is observed due to the polymer−wall interaction when D/L_0 is near or less than 3.0. A typical example can be seen in the TEM image of a particle with a single lamella in Figure 3a. For $4.0 \leq D/L_0 \leq 5.0$, an intermediate morphology

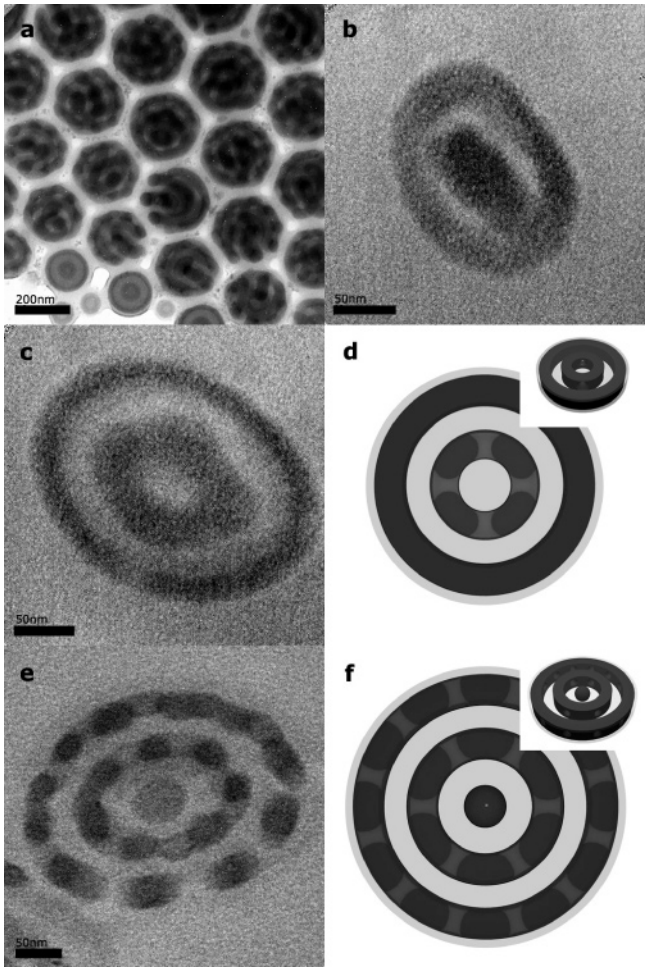

Figure 2. Blend particles of PS-*b*-PB and 10k-*h*PS for $\phi = 0.34$. (a) Blend particles were arranged by size from bottom to top. (b) One and a half bilayers with PB as the core are shown ($D/L_0 \sim 3$). (c) Intermediate structure of two bilayers with PS as the core is shown ($D/L_0 \sim 4$). (e) Perforated lamellar morphology is shown ($D/L_0 \sim 5$). (d,f) Schematic illustrations of (c) and (e) and insets in (d) and (f) are the illustrative 3D structures of (c) and (e), respectively.

similar to a cagelike network structure forms, as shown in Figure 3b. When D/L_0 exceeds 5.0, helices begin to appear in the blend particles. A few tilted TEM images of blend particles at various angles for $D/L_0 \sim 6.0$ are reproduced in Figure 3c,d. As in regions A_2 of Figure 3d and B_1 of Figure 3c, helical cylinders at the edge are perpendicular to the TEM image plane and off the normal axis in regions A_1 of Figure 3c and B_2 of Figure 3d. Therefore, we have confirmed that PB helices can form in a spherical geometry. For $D/L_0 \sim 5.5$, helices were also observed in the particles, as shown in Figure 3e. However, the axes of the helices are twisted, even though the weight fraction of *h*PS ϕ is the same as that for Figure 3c. This is because the feature spacing L_0 is not commensurate with the size of the confining geometry D. In the emulsion-based synthesis, the shape of the particles depends on the two competing contributions: one from the compressive capillary forces that are spherically symmetric and the other from the free energy associated with microdomain morphology inside the particles. The capillary forces are larger for smaller drops, and the free energy contribution depends on the structures of microdomains. For example, the blend particles of PS-*b*-PB and 10k-*h*PS for $\phi = 0.40$ remain spherical for $D/L_0 < 10.0$. Interestingly, when D/L_0 is increased above, the blend particles are either spherical or slightly elongated depending on the internal arrangement of helical microdomains, as noted for the TEM images in Figure 3f,g. In Figure 3f, the helices in an ellipsoidal particle are aligned along the main axis of the particle for $D/L_0 \sim 17$, in which L_0 is the length of the minor axis. In contrast, the orientation of helices is irregular in the spherical particle in Figure 3g for $D/L_0 \sim 17$. This implies that hexagonally packed helices prefer anisotropic ellipsoidal confinement rather than spherical confinement because spherical curvature imposes a high entropy penalty on the polymer chains. By changing the overall shape from spherical to ellipsoidal, the curvature is reduced locally near the side walls and increased near both ends of the major axes of the ellipsoids. However, the entropy penalty at the end regions can be outweighed by the entropy gain from the side regions. Meanwhile, for $D/L_0 < 10$, sphericity remained due to the dominant restoring capillary force for small D relative to the entropy-driven deforming force for ordered stacking of microdomains.

When the weight fraction of *h*PS is in the range $0.50 \leq \phi \leq 0.54$, well-stacked hoops and disks self-organize inside the blend particles for $D/L_0 \leq 7.0$. In this range of ϕ, the internal structures are strongly dependent on D/L_0, as shown in Figure 4a−d, in which the TEM images of the blend particles are reproduced for $\phi = 0.51$ with various D/L_0 ratios. As noted for Figure 4a, only one spherical PB domain is present for $D/L_0 \sim 2$. However, when $2.5 \leq D/L_0 \leq 7.0$, oblates and hoops coexist in the blend particles, and the numbers of oblates and hoops increase with D/L_0, as shown in Figure 4b−d.

As mentioned previously, the particles deform into anisotropic ellipsoids to accommodate the internal arrangement of the microphase domains with a packing structure that depends on D/L_0. The shape deformation arises because spherical confinement with diameter D is not commensurate with the ordered packing of hoops or helices with a specific feature spacing L_0. For example, the blend particles containing circular hoops with $D/L_0 \sim 7.0$ in Figure 4d are elongated due to the internal stacking of the hoops. However, for $7 < D/L_0 < 15$, helices form in the spherical particles, as shown in Figure 4e. This result implies that there is a minimum droplet volume above which helices are energetically more favorable over hoops due to their lower interface curvatures. If D/L_0 is increased further above 15, the blend particles are spherical, with PB domains coiled with irregular directional orientation, as shown in Figure 4f. The irregular coiled morphology forms to accommodate the spherical shape.

To investigate their internal morphologies in more detail, we obtained the cross-sectional images of the particles with stacked hoops and circular helices that are shown in parts a and d of Figure 5, respectively. Parts b and e of Figure 5 also show schematic illustrations of the stacked hoops and helices in the blend particles, respectively, and the thin midplane arrangements are shown in parts c and f of Figure 5, respectively. Hexagonal arrays of PB domains in the outer region and connections in the central region can be clearly observed in Figure 5a,d although the particles were distorted during the microtoming process. The cylinders in the central area in Figure 5f are parallel to one of the hexagon sides, which is not the case in Figure 5c.

When the weight fraction of *h*PS is increased further above 0.56, the PB blocks form spherical domains inside the block copolymer spheres, as shown in Figure 6, in which TEM images of the blend particles are reproduced for three different values of ϕ, 0.7, 0.8, and 0.9. As noted above, the packing of the spherical domains becomes sparser with increases in ϕ, while the size of the spherical domains is kept constant.

The observed phase morphologies for $r < 1$ are summarized in the phase diagram in Figure 6d, in which phase behavior for the block copolymer particles with *h*PS is plotted in the phase

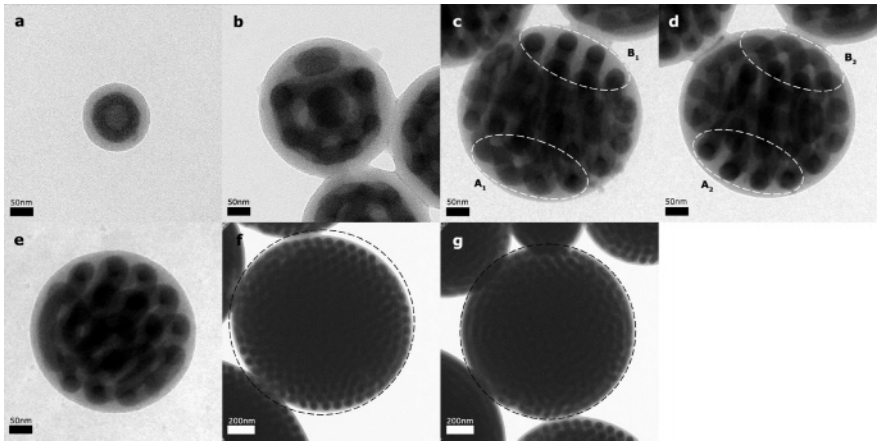

Figure 3. Blend particles of PS-*b*-PB and 10k-*h*PS for $\phi = 0.40$. (a) One lamellar layer in a particle for $D/L_0 \sim 3.0$. (b) One oblate spheroid and a cagelike network in a particle for $D/L_0 \sim 4.3$. (c) Particle in which helices are aligned for $D/L_0 \sim 6.0$. (d) Tilted image of (c). (e) Particle in which helices are not aligned for $D/L_0 \sim 5.5$. (f) Ellipsoidal particle with aspect ratio of about 1.1 for $D/L_0 \sim 17$. (g) Spherical particle for $D/L_0 \sim 17$. Dotted spherical lines in (f) and (g) represent spheres enclosing the microstructured blend particles.

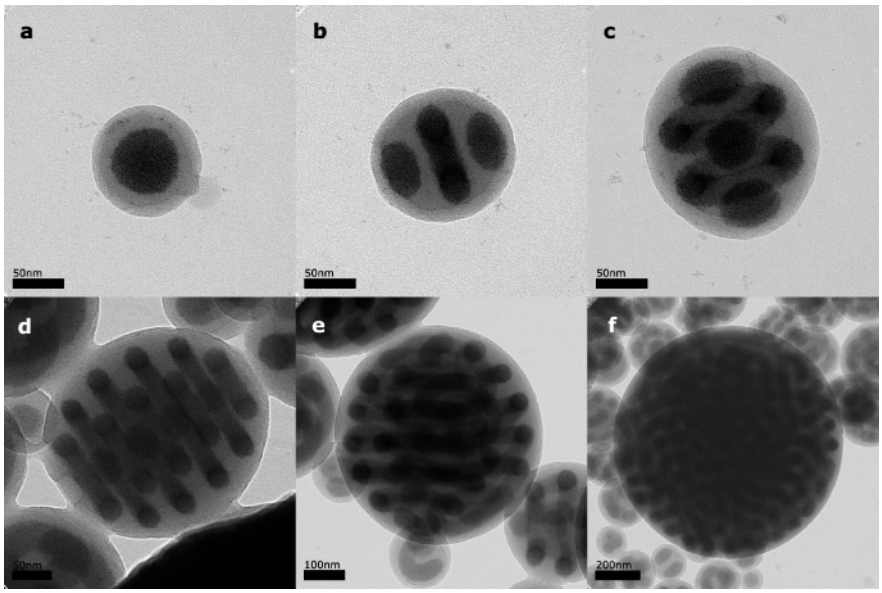

Figure 4. Blend particles of PS-*b*-PB and 10k-*h*PS for $\phi = 0.51$. (a) One spherical domain of PB blocks in a particle for $D/L_0 \sim 2.0$. (b) Two disks and one hoop in a particle for $D/L_0 \sim 2.5$. (c) Three disks and two hoops in a particle for $D/L_0 \sim 3.3$. (d) Several disks and hoops in a particle for $D/L_0 \sim 7.0$. (e) Helices in a particle for $D/L_0 \sim 10$. (f) Irregularly coiled PB domains for $D/L_0 \sim 15$.

plane D versus ϕ. The PS homopolymer induces morphological transitions from lamellae (L) to cylinders (C) and cylinders to spheres (S). Further, the perforated lamellar phase (PL) is produced in the compositional windows between the lamellar and the cylindrical domains. The particle size D also induces morphological transitions and affects the directional orientation of the cylindrical phase.

3.2. Phase Behavior of the Blend Microspheres for $r > 1$. In spin-cast films of diblock copolymers and homopolymers, macrophase separation can be induced with microphase-separated domains of block copolymer in the homopolymer matrix when the molecular weight of the homopolymer is higher than that of the corresponding chains of the diblock copolymer.[24−26,30] Here, we observed phase behavior in the blend particles of PS-*b*-PB block copolymer with 96k-*h*PS and 200k-*h*PS, i.e., $r \sim 2$ and 4, respectively. In the confining geometry, the occurrence of macrophase separation depends on r and ϕ. For $r \sim 2$, the blend of block copolymers with *h*PS forms lamellar structures for the entire range of ϕ. In the low *h*PS content limit of $\phi \leq 0.3$, onion-like particles similar to those shown in the TEM image in Figure 1a are created from the spherical confining geometry without displaying macrophase separation. For $\phi \geq 0.32$, however, macrophase separation occurs and the layer-by-layer structure is highly distorted, as shown in Figure 7. This is because the PS homopolymers (96k-*h*PS) segregate randomly at high weight fractions. In particular, for $\phi = 0.5$, the number of lamellae increases with the particle size D and whether the outermost layer is completely closed or not is sensitive to D, as can be clearly seen in Figure 7a−d. In most cases, the outermost lamella of PB blocks is significantly deformed and looks domelike. In some cases, the layer-by-layer structure is preserved with eccentric closed lamellae, as shown in Figure 7c for $D = 420$ nm. One possible explanation on such deformed layer or domelike morphologies is kinetic and stability effects. Because of the high molecular weight of *h*PS, the final morphologies would possibly be trapped in out-of-equilibrium, metastable morphologies depending on the solvent nature and evaporation process. This is especially true of high *h*PS content limits. Indeed, our results show that, when the content of 96k-*h*PS is below the onset point of macrophase separation, the blend particles have an equilibrium, symmetric morphology of concentric closed lamellae.

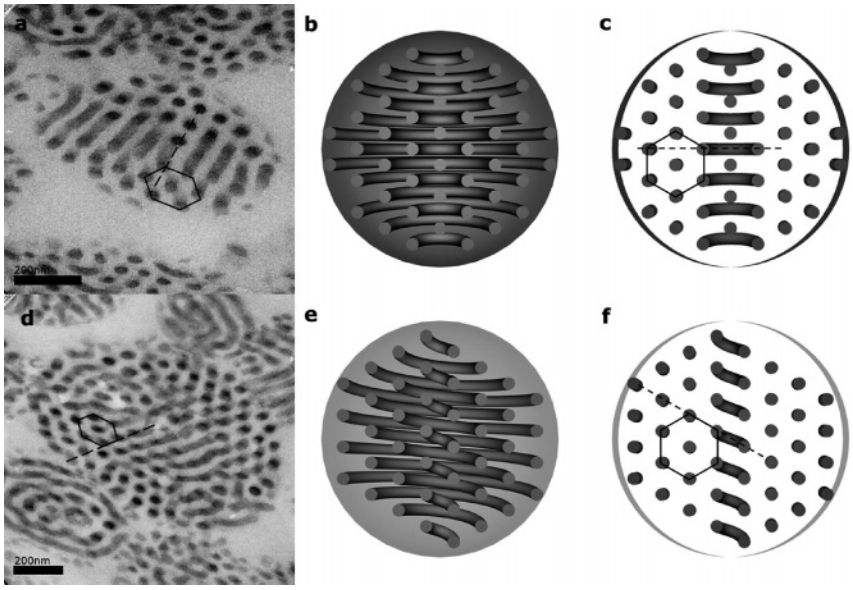

Figure 5. (a,d) TEM images of the cryomicrotomed particles with internal domains of hoops and helices, respectively, for $\phi = 0.5$. (b,e) Schematic illustrations of hoops and helices in the half spheres, respectively. (c,f) Schematic illustrations of thin midplane sections of (a) and (d), respectively.

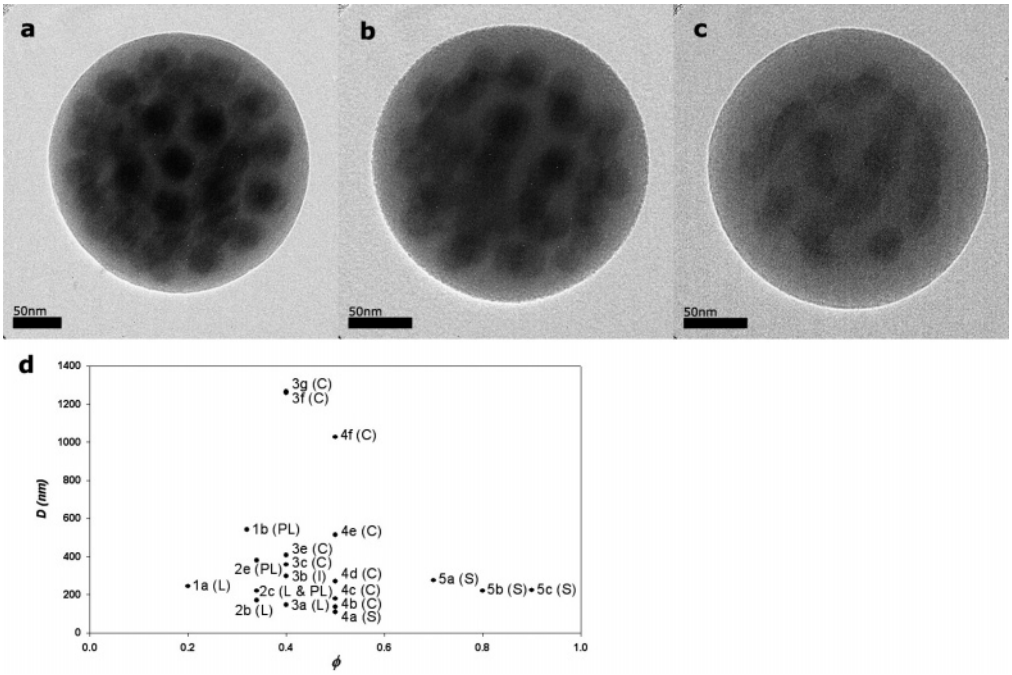

Figure 6. Blend particles of PS-*b*-PB and 10k-*h*PS. (a) Spherical domains of PB blocks are densely packed in a particle for $\phi = 0.7$ ($D = 275$ nm). (b) Number of spherical domains becomes smaller than (a) for $\phi = 0.8$ ($D = 220$ nm). (c) Small number of spherical domains are observed in a particle for $\phi = 0.9$ ($D = 223$ nm). (d) Phase morphologies are summarized for $r < 1$ in phase plane D vs ϕ. L, PL, C, and S designate lamella, perforated lamella, cylinder, and sphere microdomain morphologies, respectively. I designates an intermediate morphology between L and C.

When the weight fraction ϕ of 96k-*h*PS reaches $\phi \sim 0.7$, the PS layer becomes as thick as 100 nm and the PB layers are not deformed significantly (Figure 7e). For $\phi \sim 0.9$, only one spherical PB layer forms in the blend particle (Figure 7f). The phase diagram in Figure 7g summarizes the results for $r \sim 2$. When $r \sim 2$, only lamellar morphologies were observed over the entire range of D and ϕ in which the macrophase separation occurred.

When PS-*b*-PB block copolymers were blended with 200k-*h*PS (i.e., $r \sim 4$), lamellar structures also form over the entire range of D and ϕ, but the PS layers do not swell for $\phi \geq 0.4$. When ϕ is smaller than 0.4, the PS homopolymers of 200k-*h*PS segregate randomly in the central or peripheral regions as well as between the lamellae of the blend particles. The TEM image for $\phi = 0.3$ in Figure 8a shows blend particles with various structures according to the location of the segregated PS homopolymers. For $\phi \geq 0.4$, 200k-*h*PS segregates in the outermost region rather than inside the blend particle; typical examples are shown in Figure 8b,c for $\phi = 0.7$. In some particles, the spherical lamellae of PB domains collapse, as shown in the magnified image in Figure 8c. Note that the internal structure is strongly dependent on the feature ratio D/L_0. For example, spherical particles with an onion-like lamellar structure are produced together with particles containing collapsed lamellae for $5.8 \leq D/L_0 \leq 6.8$. Previously, homopolymer blend particles with similar internal structure were obtained by controlling interfacial tensions.[18] Specifically, when two homopolymers had an identical interfacial tension, a spherical

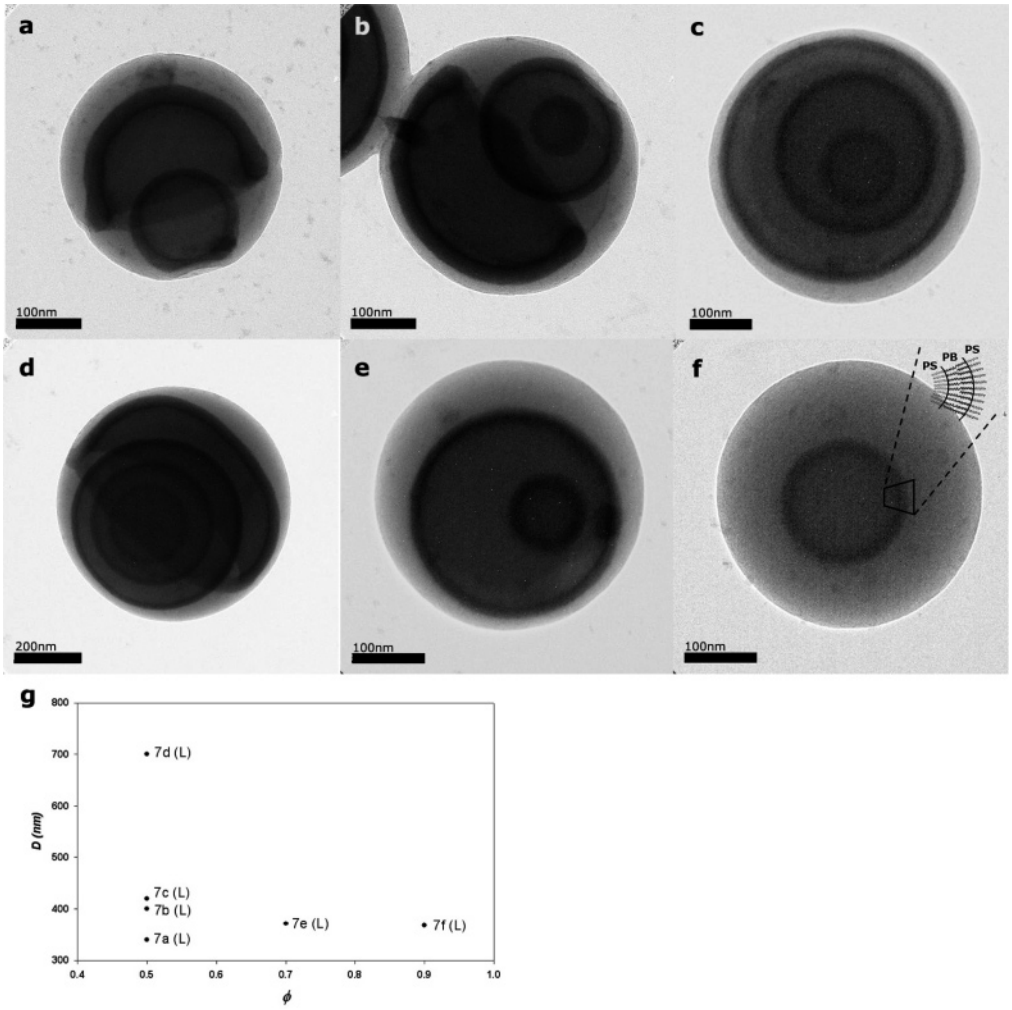

Figure 7. Blend particles of PS-*b*-PB and 96k-*h*PS. (a) One spherical lamella and one domelike lamella for $D = 340$ nm ($\phi = 0.5$). (b) Two spherical lamellae and one domelike lamella for $D = 400$ nm ($\phi = 0.5$). (c) Three nonconcentric spherical lamellae layers in a particle for $D = 420$ nm ($\phi = 0.5$). (d) Three spherical lamellae and one domelike lamella for $D \sim 700$ nm ($\phi = 0.5$). (e) Two nonconcentric spherical lamellae in a particle for $D = 371$ nm ($\phi = 0.7$). (f) Only one spherical lamella in a particle for $D = 368$ nm ($\phi = 0.9$). (g) Phase morphologies are summarized for $r \sim 2$ in phase plane D vs ϕ. L designates lamella microdomain morphology.

domain of one homopolymer protruded out from the spherical matrix of another homopolymer, resulting in asymmetric moon-shaped morphology. However, the origins of the structure formation are different because, in the present case, the asymmetric anomalous structures form due to macrophase separation. The overall phase behaviors for $r \sim 4$ are summarized in Figure 8d. Only lamellar morphologies are observed over the entire range of D and ϕ, with a lamellar spacing that is nearly independent of ϕ due to macrophase separation.

3.3. Phase Behavior of the Blend Microspheres for $r \sim 1$. We also investigated the internal morphology of blend particles of block copolymers and PS homopolymers 44k-*h*PS in the dry blush regime, i.e., $r \sim 1$. In this regime, *h*PS is also likely to be solubilized in the PS microdomains but not able to penetrate fully into the microdomain interfaces when the molecular weight of *h*PS is comparable to that of the PS block. Consequently, *h*PS is localized largely at the mid or core regions in the PS microdomains. In the absence of confining geometry, addition of *h*PS brings about only an increase in PS domain thickness without inducing microphase transition.[24−26,29] Indeed, our results show that internal lamellar structure is retained in the blend particles and addition of 44k-*h*PS leads to only an increase in PS domain thickness for $\phi \leq 0.3$. However, the morphologies change dramatically with increase in the *h*PS content ϕ above 0.32, and anomalous morphologies are produced depending on the particle size D. In Figure 9a, four particles with various particle sizes between 175 and 400 nm are shown for $\phi = 0.5$. As noted above, two small particles ($D < 250$ nm) possess lamellar structure. However, the particle with $D = 300$ nm at the bottom of Figure 9a contains both spherical and domelike lamellar structures that are similar to those in Figure 7a. As D increased to 400 nm, a microphase transition occurred in the core region of the particle, as shown in the top of Figure 9a. For larger particles ($D \sim 700$ nm), the perforation of the lamellae was clearly observed near the core region rather than in the outer region, as shown in Figure 9b. For $\phi = 0.58$, all of the lamellar layers are distorted from sphericity and have perforated cagelike morphology (Figure 9c).

When the weight fraction ϕ of *h*PS is increased further, the blend particles of a few hundred nanometers in size have various complex internal morphologies such as hoops, tetragon-like, "8"-shape, and pretzel-like structures. The base unit of these structures is a hoop, and these structures begin to form in small particles for $\phi \geq 0.7$. In Figure 10a, a single hoop inside particles can be seen for $D = 250$ nm with $\phi = 0.9$. Tetragon-like structures were produced for $D = 180$ nm ($\phi = 0.7$), as shown in Figure 10b,c, which contain TEM images at different tilted angles. Note in these TEM images that the structure consists of

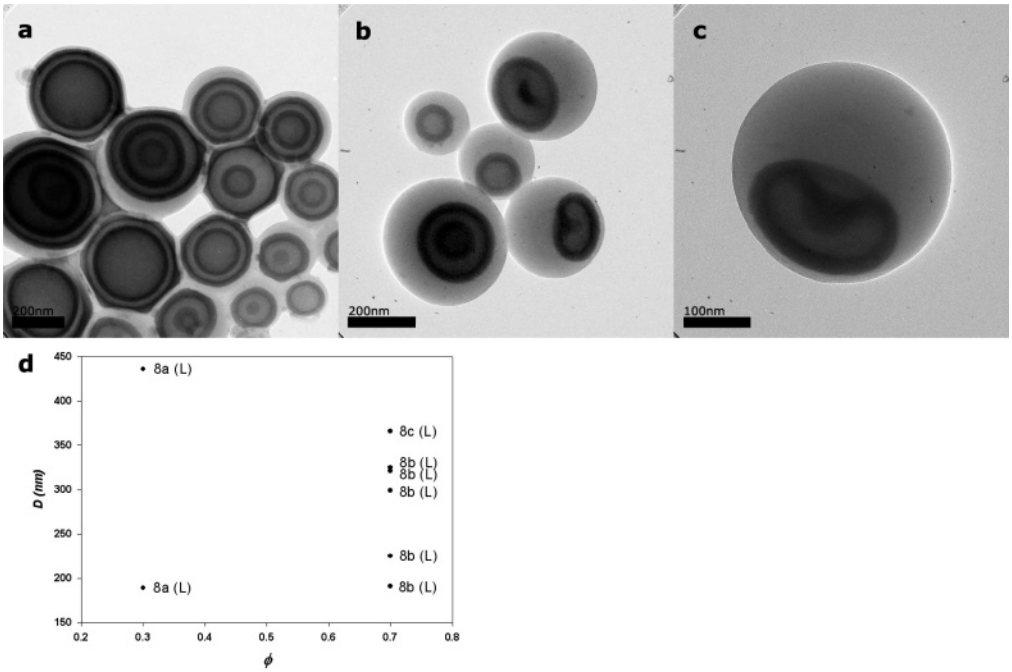

Figure 8. Blend particles of PS-*b*-PB and 200k-*h*PS. (a) Expansion of PS domain is highly irregular due to randomly segregated 200k-*h*PS ($\phi = 0.3$). (b) Particles in which the number of lamellae is two and less ($\phi = 0.7$). (c) Magnified image of collapsed lamellar layer ($\phi = 0.7$). (d) Phase morphologies are summarized for $r \sim 4$ in phase plane D vs ϕ. L designates lamella microdomain morphology.

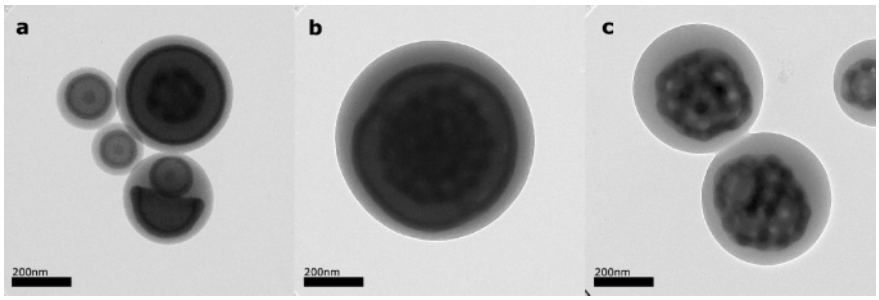

Figure 9. Blend particles of PS-*b*-PB and 44k-*h*PS. (a) Various morphologies due to the frustration or perforation of lamellae in particles for D between 175 and 400 nm ($\phi = 0.50$). (b) Perforated lamellae in a particle for $D = 670$ nm ($\phi = 0.50$). (c) Deformed perforated lamellar structure for $D = 440$ nm ($\phi = 0.58$).

two piled hoops. Similarly, the "8"-shape structure in Figure 10d for $D = 375$ nm consists of two jointed hoops in the same plane, and the pretzel-like structure in Figure 10e for $D = 400$ nm consists of triangularly jointed hoops in the same plane. A number of different structures made up of assemblies of multiply jointed hoops were also observed for blend particles with various D and ϕ.

For $r \sim 1$, L, PL, and C phases were produced in the blend particles, as summarized in the phase diagram in Figure 10f. Over a broad range of D and ϕ, several anomalous morphologies such as multiply jointed hoops were observed due to the combined effects of micro- and macrophase separations. Both L and PL phases were observed together in the phase transition from L to PL phases, and the phase transitions began at the innermost layer.

3.4. Thickness of the Swelled PS Domains in the Block Copolymer Particles. We measured the thickness (T_s) of the PS domains in the lamellar structures using an image analysis software (Gatan, Digital Micrograph); the average thickness is plotted as a function of ϕ for $\phi \leq 0.3$, with error bars in Figure 11. For $r < 1$, T_s was measured up to $\phi = 0.28$ because a phase transition occurs above $\phi = 0.30$. As expected, T_s increases with increases in the molecular weight ratio r, and the rate of increase in T_s with ϕ is higher for $r > 1$ than for $r < 1$. As previously reported, in the wet-rush regime ($r \sim 0.2$), low-molecular-weight *h*PS can more readily penetrate into the PS block domain and the lateral swelling of the PS block is more likely than domain thickness expansion. Therefore, the domain thickness is slightly increased with increase in the *h*PS content ϕ up to 0.28. On the other hand, for $r \sim 2$ and $\phi \leq 0.3$, the high-molecular-weight *h*PS localizes in the mid or core region of the PS domains without experiencing macrophase separation and the domain thickness expansion is predominant.[24−27,29,30] Similarly, for $r \sim 1$ and $\phi \leq 0.3$, *h*PS does not cause microphase transition but only increases the domain thickness. The rate of increment is intermediate between the cases of $r \sim 0.2$ and $r \sim 2$.

4. Conclusions

Block copolymer particles of PS-*b*-PB with *h*PS were successfully generated with the emulsion-based method. Spherical particles were found to be predominant due to the isotropic surface tension of the emulsion droplets, which provide spherical confinement for the self-assembly of block copolymer nanostructures. We investigated the phase behavior systematically by observing the morphologies inside the blend particles of PS-*b*-PB with *h*PS for three different ranges of r, namely $r < 1$, $r > 1$, and $r \sim 1$.

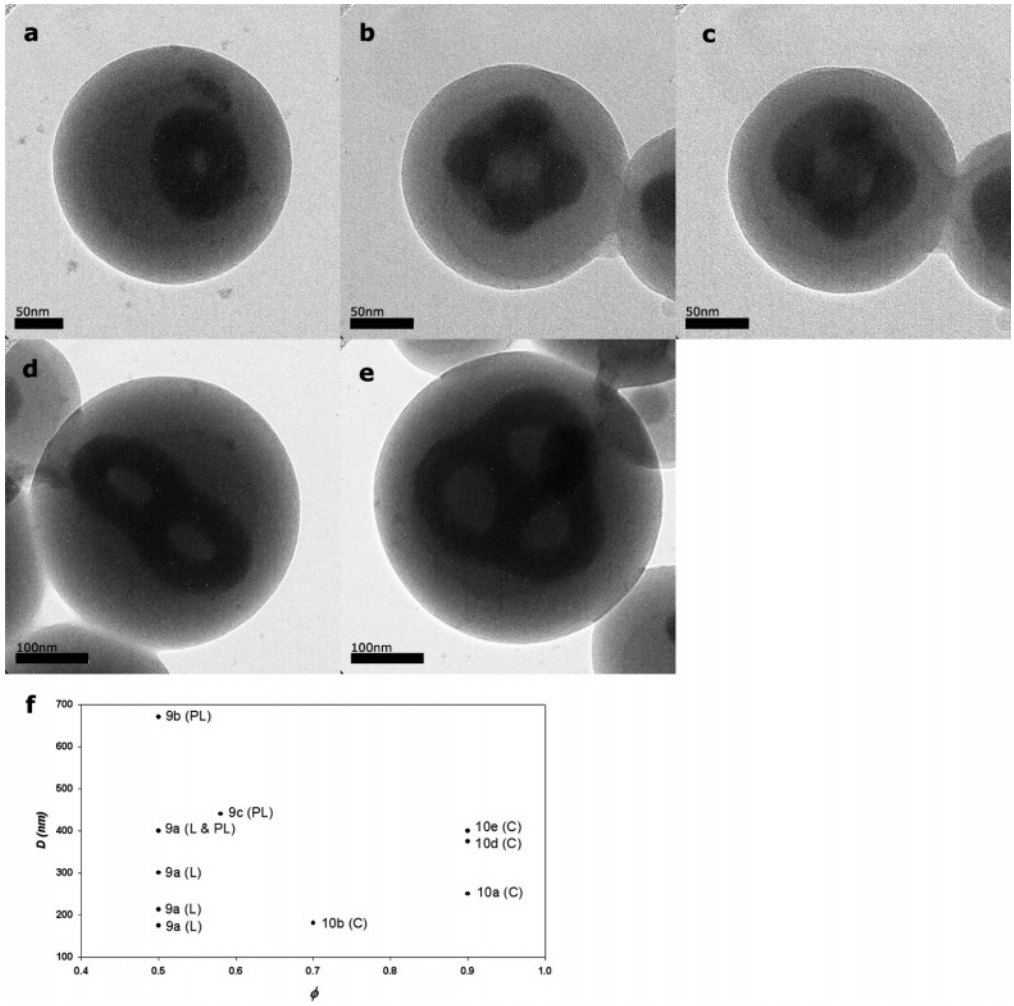

Figure 10. Blend particles of PS-*b*-PB and 44k-*h*PS. (a) Hoop in a particle for $\phi = 0.9$ ($D = 250$ nm). (b) Two hoops are piled up for $\phi = 0.7$ ($D = 180$ nm). (c) Tilted image of (b). (d) Two hoops are jointed in the same plane for $\phi = 0.9$ ($D = 375$ nm). (e) Three hoops are jointed for $\phi = 0.9$ ($D = 400$ nm). (f) Phase morphologies are summarized for $r < 1$ in phase plane D vs ϕ. L, PL, and C designate lamella, perforated lamella, and cylinder microdomain morphologies, respectively.

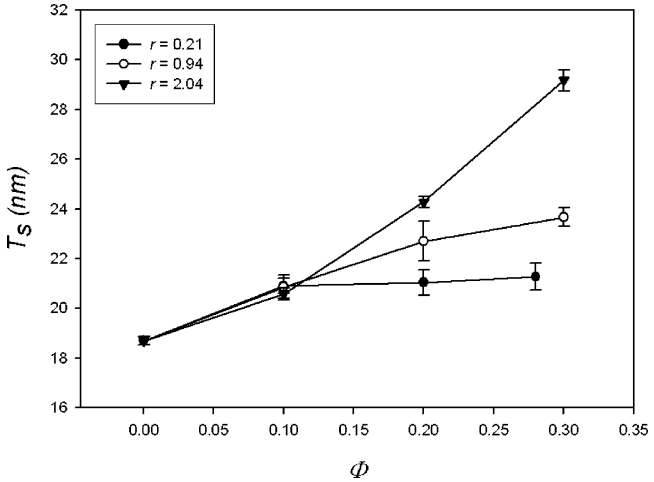

Figure 11. Growth of PS domain thickness (T_s) as a function of the weight fraction of *h*PS (ϕ) for various molecular weight ratios.

For $r < 1$, several microphase separated structures were observed, from lamellar to sphere morphologies, with increases in ϕ, similar to the morphologies of cast films. For $D/L_0 < 15$, cylindrical domains of PB blocks are produced in the form of circular helices or stacked hoops. In this case, the blend particles deform to accommodate the ordered regular packing of cylindrical domains in the confining geometry. For $r \sim 1$, complex structures consisting of spherical lamellae, domelike lamellae, perforated lamellae, and hoops are produced due to the combined effects of micro- and macrophase separations. In particular, for $\phi \geq 0.7$, hoop-based anomalous nanoscopic structures such as multiply jointed hoops form.

For $r \sim 2$, only lamellar morphologies were observed for the entire range of ϕ. For $\phi \geq 0.32$, domelike lamellar layers form in the outer region in small particles due to the segregation of *h*PS. For $r \sim 4$, an onion-like structure of block copolymer was also observed for the entire range of ϕ, with an interlayer spacing that is nearly independent of ϕ due to macrophase separation.

Our experimental observations are of fundamental significance both for understanding the phase behavior of block copolymers in confining geometries and for various applications. For instance, onion-like particles are potentially useful for dielectric resonators and spherical photonic crystals.[31] Particles with internal isolated regions are of practical importance because they can be used as new types of ideal compartments in controlled drug delivery systems. For practical applications, however, we have to employ microfluidic devices[32,33] for generating monodisperse emulsion drops, which in turn yield blend particles with all identical internal pattern of the polymer domains.

Acknowledgment. This work was supported a grant from the Creative Research Initiative Program of the Ministry of Science and Technology for "Complementary Hybridization of Optical and Fluidic Devices for Integrated Optofluidic Systems." Partial support from the Brain Korea 21 program is also appreciated. We thank Korea Basic Science Institute for allowing us to use their cryo-ultramicrotome (Leica, EMFCS).

References and Notes

(1) Bates, F. S. *Science* **1991**, *251*, 898.
(2) Fredrickson, G. H.; Bates, F. S. *Annu. Rev. Mater. Sci.* **1996**, *26*, 501.
(3) Spatz, J. P. *Angew. Chem., Int. Ed.* **2002**, *41*, 3359.
(4) Taton, T. A.; Mirkin, C. A.; Letsinger, R. L. *Science* **2000**, *289*, 1757.
(5) Hawker, C. J.; Russell, T. P. *MRS Bull.* **2005**, *30*, 952.
(6) Huang, E.; Russell, T. P.; Harrison, C.; Chaikin, P. M.; Register, R. A.; Hawker, C. J.; Mays, J. *Macromolecules* **1998**, *31*, 7641.
(7) Kikuchi, M.; Binder, K. *Europhys. Lett.* **1993**, *21*, 427.
(8) Kikuchi, M;, Binder, K. *J. Chem. Phys.* **1994**, *101*, 3367.
(9) Shin, K.; Xiang, H.; Moon, S. I.; Kim, T.; McCarthy, T. J.; Russell, T. P. *Science* **2004**, *306*, 76.
(10) Xiang, H.; Shin, K.; Kim, T.; Moon, S. I.; McCarthy, T. J.; Russell, T. P. *Macromolecules* **2004**, *37*, 5660.
(11) Wu, Y.; Cheng, G.; Katsov, K.; Sides, S. W.; Wang, J.; Tang, J.; Fredrickson, G. H.; Moskovits, M.; Stucky, G. D. *Nat. Mater.* **2004**, *3*, 816.
(12) Sun, Y.; Steinhart, M.; Zschech, D.; Adhikari, R.; Michler, G. H.; Gösele, U. *Macromol. Rapid Commun.* **2005**, *26*, 369.
(13) He, X.; Song, M.; Liang, H.; Pan, C. *J. Chem. Phys.* **2001**, *114*, 10510.
(14) Sevink, G. J. A.; Zvelindovsky, A. V.; Fraaije, J. G. E. M.; Huinink, H. P. *J. Chem. Phys.* **2001**, *115*, 8226.
(15) Feng, J.; Ruckenstein, E. *Macromolecules* **2006**, *39*, 4899.
(16) Yu, B.; Sun, P.; Chen, T.; Jin, Q.; Ding, D.; Li, B. *Phys. Rev. Lett.* **2006**, *96*, 138306.
(17) Li, W.; Wickham, R. A.; Garbary, R. A. *Macromolecules* **2006**, *39*, 806.
(18) Sundberg, D. C.; Durant, Y. G. *Polym. React. Eng.* **2003**, *11*, 379.
(19) Pham, H. H.; Gourevich, I.; Oh, J. K.; Jonkman, J. E. N.; Kumacheva, E. *Adv. Mater.* **2004**, *16*, 516.
(20) Gourevich, I.; Field, L. M.; Wei, Z.; Paquet, C.; Petukhova, A.; Alteheld, A.; Kumacheva, E.; Saarinen, J. J.; Sipe, J. E. *Macromolecules* **2006**, *39*, 1449.
(21) Babin, V.; Garstecki, P.; Holyst, P. *J. Appl. Phys.* **2003**, *94*, 4244.
(22) Reffner, J. R. Ph.D. Thesis, University of Massachusetts, Amherst, MA, 1992.
(23) Okubo, M.; Saito, N.; Takekoh, R.; Kobayashi, H. *Polymer* **2005**, *46*, 1151.
(24) Hamley, I. W. *The Physics of Block Copolymers*; Oxford University Press: New York, 1998; p 332.
(25) Matsen, M. W. *Macromolecules* **1995**, *28*, 5765.
(26) Hashimoto, T.; Tanaka, H.; Hasegawa, H. *Macromolecules* **1990**, *23*, 4378.
(27) Tanaka, H.; Hasegawa, H.; Hashimoto, T. *Macromolecules* **1991**, *24*, 240.
(28) Saito, N.; Takekoh, R.; Nakatsuru, R.; Okubo, M. *Langmuir* **2007**, *23*, 5978.
(29) Disko, M. M.; Liang, K. S.; Behal, S. K.; Roe, R. J.; Jeon, K. J. *Macromolecules* **1993**, *26*, 2983.
(30) Pan, T.; Huang, K.; Balazs, A. C.; Kunz, M. S.; Mayes, A. M.; Russell, T. P. *Macromolecules* **1993**, *26*, 2860.
(31) Urbas, A. M.; Maldovan, M.; De Rege, P.; Thomas, E. L. *Adv. Mater.* **2002**, *14*, 1850.
(32) Yi, G.-R.; Thorsen, T.; Manoharan, V. N.; Hwang, M.-J.; Jeon, S.-J.; Pine, D. J.; Quake, S. R.; Yang, S.-M. *Adv. Mater.* **2003**, *15*, 1300.
(33) Yi, G.-R.; Manoharan, V. N.; Klein, S.; Brzezinska, K. R.; Pine, D. J.; Lange, F. F.; Yang, S.-M. *Adv. Mater.* **2002**, *14*, 1137.

MA0712302